

# Mechanical properties of Ce-TZP/ $\text{Al}_2\text{O}_3$ ceramic composites as a function of sintering parameters

B. X. Freitas<sup>1\*</sup>, E. T. Duarte<sup>2</sup>, J. E. A. Vasconcelos<sup>3</sup>, R. O. Magnago<sup>2</sup>, K. Strecker<sup>4</sup>, C. Santos<sup>2</sup>

<sup>1</sup>Federal University of Itajubá, Institute of Mechanical Engineering, Itajubá, MG, Brazil

<sup>2</sup>Rio de Janeiro State University, Faculty of Technology, Resende, RJ, Brazil

<sup>3</sup>Fluminense Federal University, Faculty of Dentistry, Nova Friburgo Health Institute, Nova Friburgo, RJ, Brazil

<sup>4</sup>São João Del Rey Federal University, São J. Del Rey, MG, Brazil

## Abstract

Ceramic composites based on Ce-TZP/ $\text{Al}_2\text{O}_3$ /H6A were sintered in order to promote grain growth and to study the effects of  $\text{ZrO}_2$  grain size on the properties of this material. A mixture of  $\text{ZrO}_2$ - $\text{CeO}_2$ - $\text{Al}_2\text{O}_3$  powders was sintered at 1450 °C-2 h, following the manufacturer's recommendations. Then, the samples were further treated at 1500 or 1600 °C, for 0, 2, 8, or 24 h. The sintered specimens were characterized by X-ray diffraction, relative density, and grain size distribution. Vickers nanohardness, Young's modulus (E), and fracture toughness were measured. The materials showed complete densification for all sintering conditions studied. t- $\text{ZrO}_2$ ,  $\alpha$ - $\text{Al}_2\text{O}_3$ , and cerium hexaluminat (H6A) were observed. The alumina and hexaluminat grains had average grain sizes of 0.7 and 4.5  $\mu\text{m}$  ( $\text{AR}>3$ ), respectively, without significant variations during the additional heat treatments. However, significant growth took place for the  $\text{ZrO}_2$  grains with increasing temperature and holding time, increasing the average grain size from 0.6-1.4  $\mu\text{m}$ , when sintered at 1500 °C-2 h to 1600 °C-24 h, respectively. The materials exhibited Vickers nanohardness of 1800 HV and  $E=241\pm 15$  GPa. On the other hand, the considerable grain growth of the  $\text{ZrO}_2$  grains as a function of holding time reflected in a reduction of the fracture toughness, which decreased from 8.5 to 5.7  $\text{MPa}\cdot\text{m}^{1/2}$  for samples sintered at 1500 °C-2 h to 1600 °C-24 h, respectively.

**Keywords:** Ce-TZP/ $\text{Al}_2\text{O}_3$ /H6A composites, densification, grain growth, mechanical properties.

## INTRODUCTION

Ceramic materials based on tetragonal zirconia stabilized with 3 mol% of  $\text{Y}_2\text{O}_3$  (also known as 3Y-TZP) are among the most promising structural bioceramics because of their high flexural strength, fracture toughness, biocompatibility, and cellular response [1, 2]. It is known that the described mechanical properties are attributed to the martensitic transformation mechanism t $\rightarrow$ m, which occurs when a metastable tetragonal grain of  $\text{ZrO}_2$  is subjected to tensile stress, such as those promoted by the opening of a crack. This tensile stress induces the transformation of tetragonal  $\text{ZrO}_2$  (t) grains near the crack tip into monoclinic  $\text{ZrO}_2$  (m) grains, with a volumetric expansion of 3% to 5%, generating compressive stresses in the surrounding grains and, thus, reducing the tensile stress at the crack tip and increasing the fracture toughness [3, 4]. One of the major concerns in the use of these ceramics in structural applications involving humid/aqueous environments is related to the mechanical instability induced by the low-temperature hydrothermal degradation mechanism (LTD) [5]. Due to the presence of oxygen vacancies in their crystalline lattice, yttrium-stabilized tetragonal zirconia grains are susceptible to hydroxyl (OH<sup>-</sup>) penetration in humid environments and, as a result, instability of the tetragonal phase by causing expansion and favoring the t $\rightarrow$ m transformation. Furthermore, the process results in the formation of yttrium

hydroxide (Y-OH) on the surface, decreasing the overall  $\text{Y}_2\text{O}_3$  content of surface grains and altering the internal energy balance of the degraded grain until it presents the necessary energy for a spontaneous t $\rightarrow$ m transformation or under the action of mechanical stimuli of low intensity [6, 7].

Tetragonal polycrystalline zirconia stabilized with  $\text{CeO}_2$  (Ce-TZP) has shown to be an interesting alternative to 3Y-TZP ceramics, as it is biocompatible [8, 9] and exhibits also a very high fracture toughness, in the order of 9 to 14  $\text{MPa}\cdot\text{m}^{1/2}$  [10, 11], besides a reasonable bending strength of about 500 to 700 MPa. Furthermore, Ce-TZP maintains its strength even after long periods of hydrothermal degradation tests [12, 13]. This behavior occurs because of the larger  $\text{Ce}^{4+}$  ions, when compared to  $\text{Y}^{3+}$  ions, which form a solid solution with zirconia, preventing the formation of vacancies in the crystalline network and so allowing for greater stability of the tetragonal system, thus considerably increasing the resistance to hydrothermal aging of Ce-TZP compared to 3Y-TZP ceramics [14-16]. On the other hand, its flexural strength, varying between 500 and 700 MPa, is significantly lower than that of 3Y-TZP (900-1200 MPa), making a series of potential structural applications for this material unfeasible, such as flaking nozzles in steelmaking processes, or dental implants for example [17, 18]. A strategy used to improve the mechanical performance of monolithic Ce-TZP ceramics, while preserving their resistance to hydrothermal degradation, is the creation of ceramic composites containing a second phase acting as reinforcement, which should present a thermal and biological compatibility with the zirconia

\* <https://orcid.org/0000-0001-7721-7687>

matrix [19-22]. It has been shown that the reinforcement of a zirconia matrix, with submicrometric alumina ( $\text{Al}_2\text{O}_3$ ) grains, improves the flexural strength by a factor of two to three times its original value [23]. These gains are associated with increased transformation zones around a crack path associated with large compressive stresses created in the material during stress application. Although some of these works mention the presence of elongated, micrometric  $\text{Al}_2\text{O}_3$  grains in the zirconia matrix, their contribution to the material's toughness has not been explored. Furthermore, zirconia matrices containing  $\text{Ce}^{4+}$  and  $\text{Y}^{3+}$  together as tetragonal phase stabilizers have not been investigated yet.

One of the great challenges to further expand the field of application of zirconia is to improve its reliability, which can be achieved through better control and understanding of the sintering process. In this context, mastering the processes of densification and microstructural development during sintering is essential for the successful use of ceramics in structural applications. In the past, it was verified that the lack of control of the microstructural characteristics can create serious problems related to the failure of ceramics, either by exaggerated grain growth or failures related to the degradation of these ceramics. Several investigations [24-27] stated relations between grain growth of 3Y-TZP ceramics and their implications on mechanical properties. The authors studied the grain growth of stabilized 3Y-TZP ceramics starting from nanocrystalline powders with samples rapidly densified through a two-step sintering technique: pre-sintering at 1100 °C-4 h followed by hot isostatic pressing at 1350 °C-2 h [24, 25]. Then, the samples were subsequently heat treated at temperatures between 1350 and 1650 °C for 2 h. The grain sizes of the samples increased from 0.165 to 0.22, 0.33, 0.655, and 1.23  $\mu\text{m}$  after heat treatment at 1350, 1450, 1550, and 1650 °C, respectively. The grain growth exponent ( $n$ ) varied between 2 and 3 and the activation energy ( $Q$ ) calculated was 280 kJ/mol. Tekeli and Erdogan [26] sintered  $\text{ZrO}_2$  (8 mol%  $\text{Y}_2\text{O}_3$ ) at 1350 °C for 1 h, followed by thermal treatments to induce grain growth at 1400, 1500, and 1600 °C for 10, 33, and 66 h. The grain growth exponent also varied between 2 and 3 and the activation energy calculated was 290 kJ/mol. Bernard-Granger and Guizard [27] studied the densification and grain growth of a 3Y-TZP powder with nanometric size, demonstrating by dilatometry that the densification starts around 1000 °C and concludes close to 1500 °C. They observed an average grain size of the sintered samples varying between 0.12 and 0.20  $\mu\text{m}$  and determined an activation energy of 300 kJ/mol.

Although several studies report results regarding 3Y-TZP or even Ce-TZP ceramics, there are no reports of studies that correlate the effects of grain growth in Ce-TZP composites with their mechanical properties. Thus, the objective of this work was to study and compare the sintering behavior and the microstructural development of Ce-TZP/ $\text{Al}_2\text{O}_3$  ceramic composite, relating the results of densification and grain growth to the sintering conditions. Furthermore, the influence of the microstructural variations on the resulting mechanical properties has also been evaluated.

## EXPERIMENTAL

A commercial powder of  $\text{ZrO}_2$  nanoparticles, doped with 10.5 wt% of a  $\text{CeO}_2/\text{Y}_2\text{O}_3$  mixture with a proportion of 90:10, was used. Furthermore, the powder also contained 25 wt%  $\text{Al}_2\text{O}_3$  as a reinforcing agent. The main characteristics of this material are shown in Table I.

Table I - Characteristics of the raw material Ce-TZP/ $\text{Al}_2\text{O}_3$  (ZirPro Intense, Saint Gobain, France) used (manufacturer's data).

Characteristic	Value
$\text{Al}_2\text{O}_3$ (wt%)	25±1
$\text{CeO}_2/\text{Y}_2\text{O}_3(90/10)$ (wt%)	10.5±0.5
$\text{SiO}_2+\text{Fe}_2\text{O}_3+\text{Na}_2\text{O}$ (wt%)	<0.06
$\text{ZrO}_2+\text{HfO}_2$ (wt%)	Balance
Grain size D50/D90 (nm)	200/100

Disc-shaped samples with a diameter of 14 mm and 1.4 mm thickness of (Ce,Y)-TZP/ $\text{Al}_2\text{O}_3$  and 3Y-TZP were compacted using uniaxial double-acting piston pressing, under an applied pressure of 100 MPa for 60 s. The samples were sintered at 1450 °C without isothermal threshold, using a heating rate of 1 °C/min and a cooling rate of 5 °C/min. After sintering, the samples were divided into groups of 5 specimens each and re-sintered at temperatures of 1450, 1500, and 1600 °C for 2, 8, or 24 h in a furnace (F-1650, Maitec, Brazil).

The apparent density of the sintered samples was determined by the immersion method based on Archimedes' principle, using a 0.0001 g precision scale (Discovery, Ohaus). The relative density was determined using the relationship between the apparent density of the sintered samples and the theoretical density of 5.40 g/cm<sup>3</sup> for the (Ce,Y)-TZP/ $\text{Al}_2\text{O}_3$  mixture, as provided by the manufacturer. The crystalline phases were identified by X-ray diffraction analysis, using a diffractometer (Empyrean, Panalytical) with  $\text{CuK}\alpha$  radiation, varying  $2\theta$  between 20° and 80°, with an angular step of 0.02° and 90 s counting time. The crystalline phases were identified using a software (X'pert-Highscore) and comparison with the ICDS file database. Quantification of the crystalline phases was performed through Rietveld refinement using the software (Highscore plus), adopting Pseudo-Voigt curves for the peak adjustment. The microstructures were observed in a scanning electron microscope with a field emission gun (SEM/FEG, 7100FT, Jeol) coupled with an energy dispersive spectroscope (EDS, X-Max, Oxford) with an 80 mm<sup>2</sup> detector. For microstructural evaluation, the polished surfaces of the sintered specimens were thermally etched at 1420 °C for 15 min and prior to the SEM investigations, a thin layer of gold was deposited using a metallizer (K550X, Quorum Technol., UK), with a current of 30 mA for 2 min. After capturing the images, a population of approximately 500 grains per sample was analyzed using the ImageJ software. In this way, the average grain sizes and their respective standard deviations were determined.

The surfaces of the polished samples (sintering condition:

1600 °C-2 h) were submitted to nanoindentation tests, using a dynamic ultra-micro hardness tester equipped with a Berkovich diamond indenter (DUH-211S, Shimadzu, Japan), varying the maximum load between 250 and 1960 mN. Furthermore, the maximum depth of penetration in the tests was 10 µm. For each individual indentation test, care was taken to ensure that the material zone was free of pores. Using a confocal optical microscope coupled to the nanoindenter, micrographs of characteristic residual nanoindentation impressions were obtained. Using the Oliver and Pharr model [28, 29], Young's modulus was calculated. The result was obtained by the average of five nanoindentations and the error was derived from the standard deviation. Using the indentation hardness ( $H_{it}$ ), the Vickers hardness (HV) was estimated by:

$$HV = 0.0925.H_{it} \quad (A)$$

where  $H_{it}$  is the hardness measured with a Berkovich indenter ( $mN/\mu m^2$ ), given by:

$$H_{it} = \frac{F_{max}}{A_p} \quad (B)$$

where  $F_{max}$  is the maximum load and  $A_p$  is the projected contact surface, which can be calculated by:

$$A_p = 24.5.[h_{max} - 0.75(h_{max} - h_r)]^2 \quad (C)$$

where  $h_{max}$  is the maximum indentation depth (µm) and  $h_r$  the intersection points of the tangent line to the loading curve, from  $F_{max}$  with horizontal axis in relation to the indentation depth (µm). The Young's modulus (E) was calculated by:

$$E_{it} = \frac{1 - \nu_s^2}{S\sqrt{\pi} - \frac{1 - \nu_i^2}{E_i}} \quad (D)$$

where  $E=E_{it}$  is dynamic Vickers nanoindentation, S is the contact stiffness between the indenter and the sample,  $A_p$  is the contact area,  $\nu_i$  and  $E_i$  are Poisson's ratio (0.07) and Young's modulus (1140 GPa), respectively, and  $\nu_s$  was not informed to the user and was available in the equipment software. The fracture toughness of the sintered samples was determined using the Vickers indentation method [30, 31], adopting the impression measurements and the crack lengths of the pyramidal apices, using a microhardness equipment (Time Group, China). An indentation load of 1000 gF (9.8 N) was applied for 30 s during the tests. In each sample, five ( $n=5$ ) indentations were measured. The cracks present at the indentation vertices were observed under an optical microscope with a coupled image analyzer (Image IA-3001). Thus, the fracture toughness,  $K_{IC}$ , was calculated considering a Palmqvist-type crack system ( $c/a$  ratio <2.5) according to [32]:

$$K_{IC} = 0.0084 \cdot \left(\frac{E}{HV}\right)^{0.4} \cdot \left(\frac{P}{a.l}\right)^{1/2} \quad (E)$$

where E represents Young's modulus (GPa), HV the hardness (GPa), P the applied load (N), a the length of the diagonal of the impression mark, and l the length of the crack generated by the Vickers indentation mark (mm).

## RESULTS AND DISCUSSION

SEM images of the starting powder mixture and phase composition determined by X-ray diffraction analysis

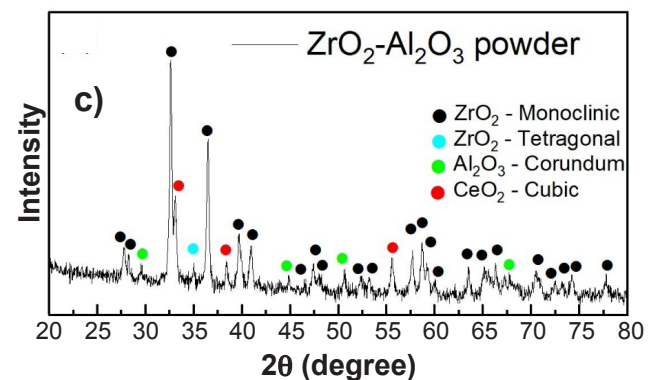
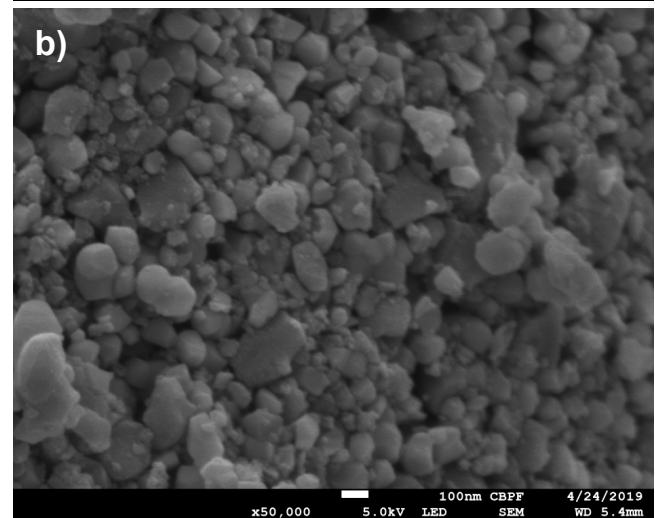
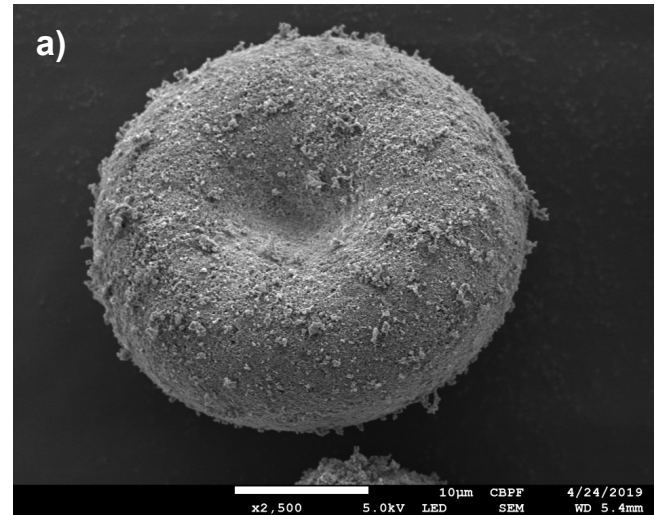


Figure 1: SEM micrographs of particles agglomerated with binding (a,b) and XRD pattern of powder (c).

are shown in Fig. 1. A semi-spherical morphology of agglomerates with sizes larger than 10  $\mu\text{m}$  was observed (Fig. 1a). The closer observation of these clusters (Fig. 1b) indicated that the agglomerates were composed of irregularly shaped particles of nanometric size. The results of XRD analysis (Fig. 1c) and their respective quantification of phases obtained by Rietveld refinement ( $\chi^2=1.14$ ) indicated that the raw material was a powder mixture consisting of 34.5% monoclinic (m)  $\text{ZrO}_2$ , 23.8%  $\text{Al}_2\text{O}_3$ , besides 9.8%  $\text{CeO}_2$  as dopant and 1.9% tetragonal (t) yttrium stabilized  $\text{ZrO}_2$  as crystalline phases.

The relative density of the samples sintered at different temperatures and isothermal holding times are shown in Fig. 2. Note that under all temperatures studied, the observed relative density was greater than 99%, ensuring a high densification of the sintered composites. The X-ray diffraction analysis results for the samples sintered at different temperatures and isothermal holding times are shown in Fig. 3. Tetragonal  $\text{ZrO}_2$  and  $\alpha\text{-Al}_2\text{O}_3$  were identified as crystalline phases. Cerium hexaluminat (H6A) has diffraction peak positions similar to  $\text{Al}_2\text{O}_3$  and lower relative intensity, which is the possible reason for its non-identification by the software, however, it was considered that it coincided with the  $\text{Al}_2\text{O}_3$  (corundum) peaks presented in Fig. 3. The significant increase in the tetragonal phase content and consequent elimination of the m- $\text{ZrO}_2$  and  $\text{CeO}_2$  phases from the initial powder mixture indicated that  $\text{Ce}^{4+}$  was absorbed in the stabilization of the tetragonal phase during the sintering of the composites. Furthermore, there were no significant changes in crystallinity as well as in phase proportions, except in samples sintered at 1600  $^\circ\text{C}$ -24 h. For this sintering condition, the presence of approximately 18.1% m- $\text{ZrO}_2$  was observed, in addition to 58% t- $\text{ZrO}_2$ , and 23.9%  $\text{Al}_2\text{O}_3$ +H6A, indicating a partial, spontaneous phase transformation of t- $\text{ZrO}_2$  occurred, which is discussed later.

Fig. 4 presents some representative SEM micrographs of the microstructures of the composites sintered at different temperatures and for different isothermal holding times.

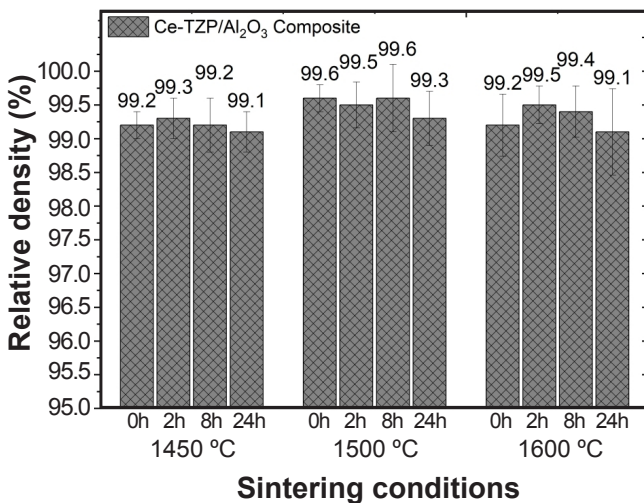


Figure 2: Relative density of samples as a function of sintering parameters.

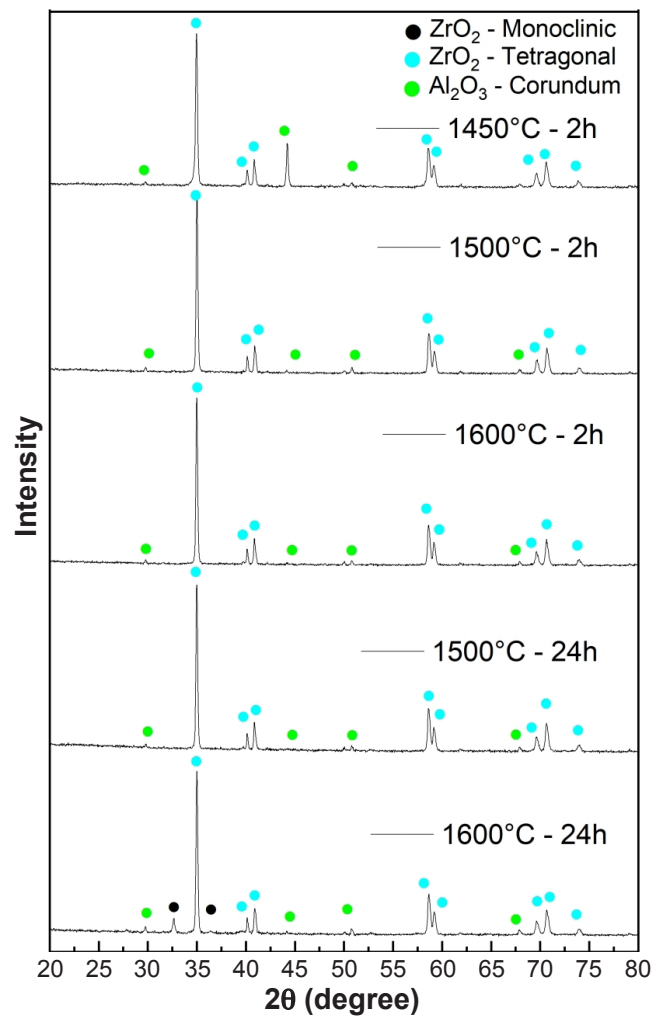


Figure 3: XRD patterns of the sintered samples for different sintering temperatures and isothermal holding times.

Fig. 5 presents the  $\text{ZrO}_2$  grain size variation in function of temperature and isothermal times. It is interesting to observe that the microstructures of the composites sintered at 1450  $^\circ\text{C}$  exhibited a matrix of spherical zirconia grains (light gray phase) with grain sizes smaller than 1  $\mu\text{m}$  and  $\text{Al}_2\text{O}_3$  grains (black phase) of spherical shape, besides large platelets with average sizes exceeding 15  $\mu\text{m}$  attributed to being cerium hexaluminat (H6A). The  $\text{Al}_2\text{O}_3$  and H6A grains had an average grain size of 0.7 and 4.5  $\mu\text{m}$ , respectively, without significant variations during the additional heat treatments. Furthermore, probably due to the low volume fraction, this phase cannot be observed in the diffractograms in Fig. 3. The formation of cerium hexaluminat consumed part of the alumina originally present in the starting powder and has been described in previous works [33]. This microstructural profile is maintained for different sintering conditions, temperatures and holding times. However, it is possible to verify differences in both phases, with increasing sintering temperature. An approach focused on the grain growth of tetragonal  $\text{ZrO}_2$  is presented in Figs. 4 and 5. It can be seen that grain growth occurred as a function of temperature and also of the isothermal holding time. At 1450 and 1500

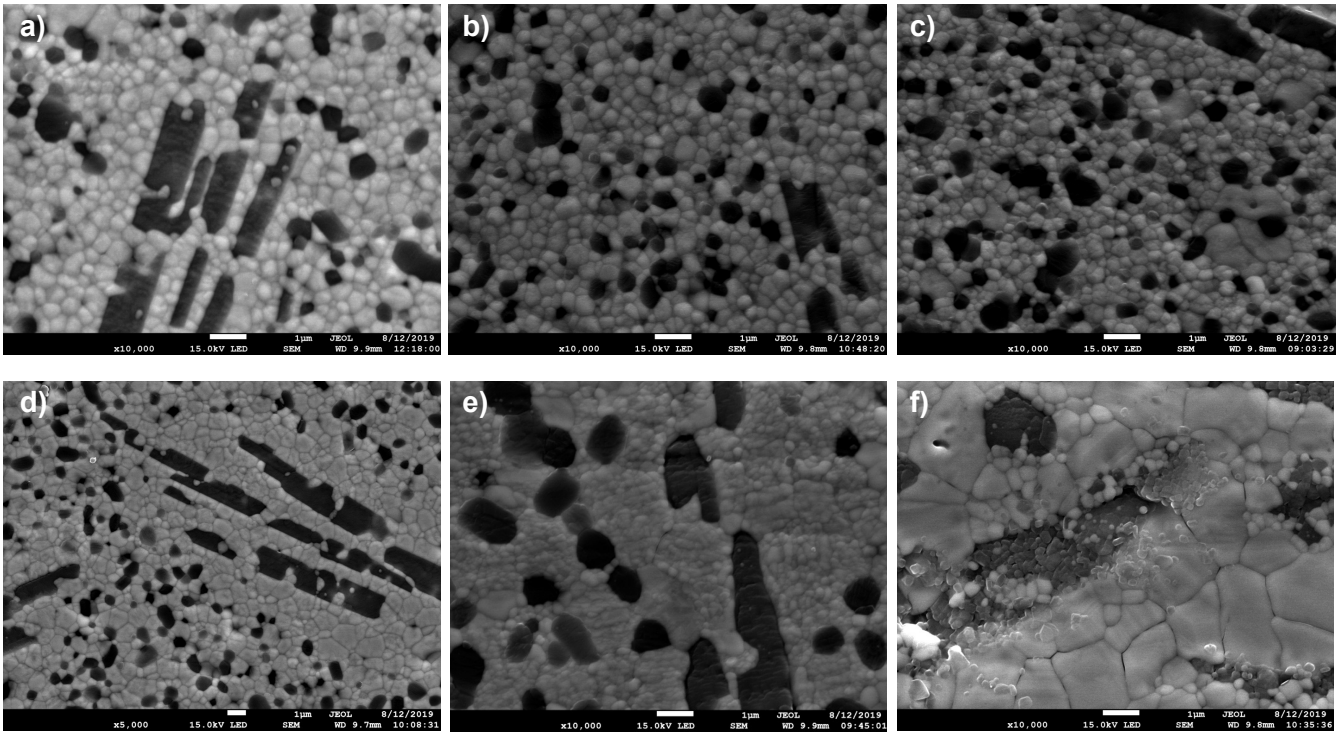


Figure 4: SEM micrographs of the samples (black regions:  $\text{Al}_2\text{O}_3$  grains and H6A platelets; white phase: zirconia grains), sintered in different conditions: a) 1450 °C, 2 h; b) 1500 °C, 2 h; c) 1600 °C, 2 h; d) 1450 °C, 24 h; e) 1550 °C, 24 h; and f) 1600 °C, 24 h.

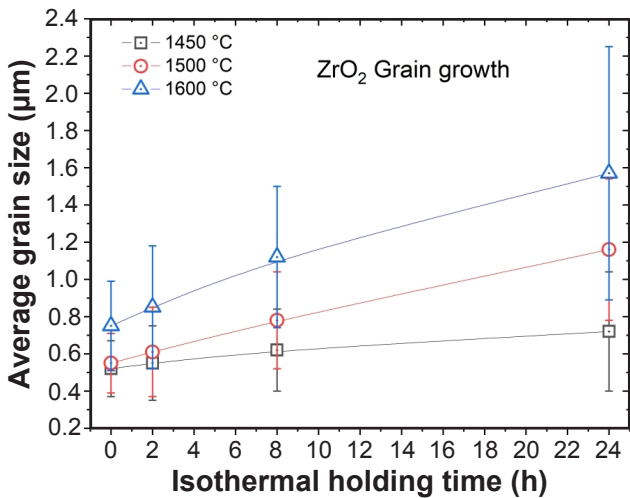


Figure 5: Average  $\text{ZrO}_2$  grain size as a function of sintering temperature and isothermal holding time.

°C, the growth of zirconia grains was not very pronounced even for prolonged isothermal treatments. In fact, at these temperatures, the diffusivity of zirconia was still low, meaning that even for an excessive holding time of 24 h of isothermal treatment, the  $\text{ZrO}_2$  grains did not grow more than a size of around 1 µm. At a higher temperature however, 1600 °C, the grain growth of zirconia was much more pronounced, exhibiting some exaggerated grain growth, more clearly for the longer isothermal holding time at 1600 °C (24 h, Fig. 4f). A tendency for a larger

grain growth of zirconia grains surrounding H6A platelets was observed. Therefore, the residual thermal stresses after sintering may be of sufficient intensity to activate the tetragonal-monoclinic transformation ( $t \rightarrow m$ ), which may explain the presence of  $m\text{-ZrO}_2$  in the diffractogram of the composite sintered at 1600 °C-24 h (Fig. 3).

Fig. 6 presents the results of Vickers hardness and modulus of elasticity obtained by nanohardness test in the sintering condition of 1600 °C-2 h (chosen because it represented the densified material without exaggerated grain growth), as well as the fracture toughness results of the composites as a function of sintering parameters. In Fig. 6a, an average Vickers hardness of  $1805 \pm 24$  HV is observed, without a well-defined profile of the effect of the indentation load on the results. This value reflected the degree of densification of the material and the influence of the alumina content in the final composition of the material. With respect to the results of the modulus of elasticity ( $E$ ), there was a tendency to reduce the absolute value of  $E$ , depending on the indentation load used. At an indentation load of 1960 mN, the average elastic modulus was  $241 \pm 15$  GPa, within the order of magnitude for alumina-toughened zirconia (ATZ) ceramic composites [34, 35]. The fracture toughness results shown in Fig. 6c indicate that this property was significantly affected by the adopted sintering parameters. Note that under lower sintering temperature conditions and without a sintering threshold (1500 °C-0 h) the average value was  $8.5 \pm 0.7$   $\text{MPa}\cdot\text{m}^{1/2}$  and the increase in sintering temperature to 1600 °C-2 h led to reductions

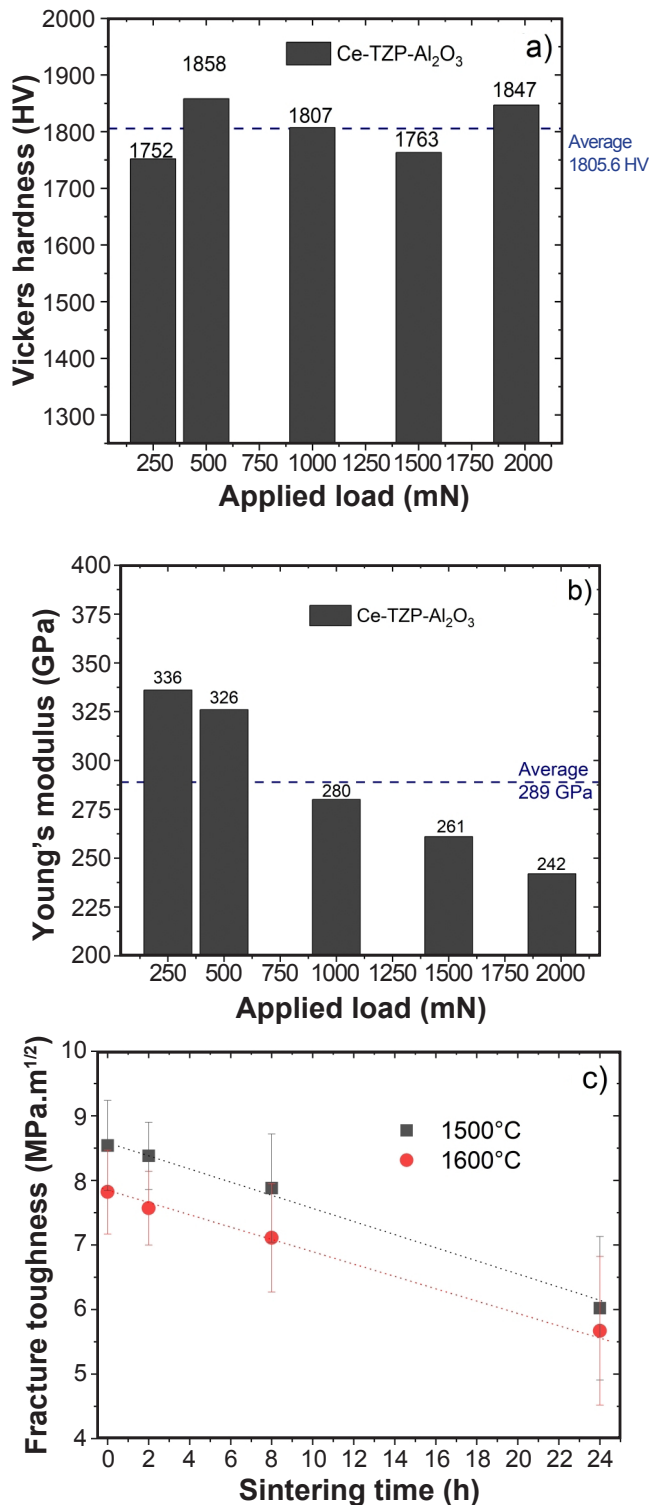


Figure 6: Hardness (a) and modulus of elasticity,  $E$  (b), of Ce-TZP/ $\text{Al}_2\text{O}_3$  composite sintered at  $1600\text{ }^\circ\text{C}$ -2 h as a function of indentation load, and fracture toughness (c) of composites sintered at different temperatures and isothermal holding times.

of almost 10% in material toughness. Increasing sintering time was more effective in reducing toughness. Under extreme sintering conditions ( $1600\text{ }^\circ\text{C}$ -24 h), there was a

33% reduction in this property, compared to the group of samples sintered at  $1500\text{ }^\circ\text{C}$ -0 h. These results reflected the considerable microstructural alteration presented by the material, which developed a heterogeneous microstructure with large grains. Thus, there was a decrease in the toughening effects during the propagation of cracks with loss of resistance of the material.

## CONCLUSIONS

Ce-TZP/ $\text{Al}_2\text{O}_3$  composites sintered at  $1500$  or  $1600\text{ }^\circ\text{C}$  present satisfactory densification results even without applying isothermal thresholds during sintering. The tetragonal zirconia grains, mostly stabilized with ceria (Ce-TZP) proved to be very sensitive to the increase in the final sintering temperature, as well as to the increase in the isothermal holding time, showing growth and with average sizes ranging from  $0.5$  to  $0.7\text{ }\mu\text{m}$  with an increase of  $100\text{ }^\circ\text{C}$  ( $1500$  to  $1600\text{ }^\circ\text{C}$ ) in the final sintering temperature. The highest grain growth rates were related to the isothermal levels, with zirconia grains with an average size close to  $1.7\text{ }\mu\text{m}$ , for sample sintered at  $1600\text{ }^\circ\text{C}$ -24 h. Under these conditions, a pronounced reduction in fracture toughness was observed and reflected a reduction in the toughening capacity of these zirconia grains in the composites. For sintering strategies that require increases in isotherm levels to obtain improvements in densification, the loss of mechanical properties must be considered.

## ACKNOWLEDGMENTS

The authors thank FAPERJ and CNPq for the financial support given to this work.

## REFERENCES

- [1] J. Chevalier, L. Gremillard, A.V. Virkar, D.R. Clarke, *J. Am. Ceram. Soc.* **92**, 9 (2009) 1901.
- [2] K.I. Afrashtehfar, M.D. Fabbro, *J. Prosthet. Dent.* **123**, 3 (2020) 419.
- [3] P.M. Kelly, L.F. Rose, *Prog. Mater. Sci.* **47**, 5 (2002) 463.
- [4] M. Guazzato, M. Albakry, S.P. Ringer, M.V. Swain, *Dent. Mater.* **20**, 5 (2004) 449.
- [5] V. Lughi, V. Sergo, *Dent. Mater.* **26**, 8 (2010) 807.
- [6] M. Yoshimura, T. Noma, K. Kawabata, S. Somiya, *J. Mater. Sci. Lett.* **6**, 4 (1987) 465.
- [7] J.J. Swab, *J. Mater. Sci.* **26** (1991) 6706.
- [8] B. Basu, *Int. Mater. Rev.* **50**, 4 (2005) 239.
- [9] A.K. Pandey, K. Biswas, *Ceram. Int.* **40**, 10 (2014) 15889.
- [10] K. Tsukuma, M. Shimada, *J. Mater. Sci.* **20** (1985) 1178.
- [11] K. Tsukuma, *Am. Ceram. Soc. Bull.* **65** (1986) 1386.
- [12] S. Bernardi-Martín, B.M. Moshtaghioun, D.G. Garcías, *J. Eur. Ceram. Soc.* **34**, 16 (2014) 4469.
- [13] M.F.R.P. Alves, M.H.F.V. Fernandes, J.K.M.B. Daguano, A.C.D. Rodas, J.E.V. Amarante, C. Santos, *J. Mech. Behav. Biomed. Mater.* **134** (2022) 105363.
- [14] R.F. Marcomini, V.L. Arantes, *Cerâmica* **67**, 382

(2021) 244.

- [15] R. Chaim, M. Hefetz, J. Mater. Sci. **39**, 9 (2004) 3057.  
[16] S. Ramesh, K.Y.S. Lee, C.Y. Tan, Ceram. Int. **44** (2018) 20620.  
[17] ISO 13356:2015, “Implants for surgery: ceramic materials based on yttria-stabilized tetragonal zirconia (Y-TZP)” (2015).  
[18] C. Sanon, J. Chevalier, T. Douillard, M. Cattani-Lorente, S.S. Scherrer, L. Gremillard, Dent. Mater. **31**, 1 (2015) 15.  
[19] N. Kajiwara, C. Masaki, T. Mukaibo, Y. Kondo, T. Nakamoto, R. Hosokawa, Implant Dent. **24**, 1 (2015) 37.  
[20] R.A. Cutler, R.J. Mayhew, K.M. Prettyman, A.V. Virkar, J. Am. Ceram. Soc. **74**, 1 (1991) 179.  
[21] J.F. Tsai, U. Chon, N. Ramachandran, D.K. Shetty, **75**, 5 (1992) 1229.  
[23] F. Kern, R. Gadow, Adv. Sci. Technol. **87** (2014) 118.  
[24] A.A. Palmeira, M.J. Bondioli, K. Strecker, C. Santos, Ceram. Int. **42**, 2 (2016) 2662.

- [25] R. Chaim, Mater. Sci. Eng. A **486**, 1-2 (2008) 439.  
[26] M.S. Tekeli, B. Erdogan, Aktas, Ceram. Int. **30** (2004) 2203.  
[27] G. Bernard-Granger, C. Guizard, J. Am. Ceram. Soc. **90**, 4 (2007) 1246.  
[28] W.C. Oliver, G.M. Pharr, J. Mater. Res. **7** (1992) 1564.  
[29] W.C. Oliver, G.M. Pharr, J. Mater. Res. **19** (2004) 3.  
[30] ASTM C1327-15, “Standard test method for Vickers indentation hardness of advanced ceramics”, ASTM Int. (2019).  
[31] C1421-10, “Standard test methods for determination of fracture toughness of advanced ceramics at ambient temperature”, ASTM Int. (2010).  
[32] K. Niihara, J. Mater. Sci. Lett. **2** (1983) 221.  
[33] F. Kern, Ceramics **3** (2020) 190.  
[34] E. Gregorová, L. Semrádová, I. Sedlářová, V. Nečina, S. Hříbalová, W. Pabst, J. Eur. Ceram. Soc. **41**, 6 (2021) 3559.  
[35] V. Tebaldo, G. Gautier, Ceram. Int. **39**, 3 (2013) 2683.  
(Rec. 11/07/2023, Rev. 26/09/2023, Ac. 20/10/2023)

